Proceedings of ASME Turbo Expo 2011
GT2011
June 6-10, 2011, Vancouver, British Columbia, Canada

GT2011-45076

Aerodynamic Optimisation of a Centrifugal Compressor Return Channel and U-turn with Genetic Algorithms

A. Hildebrandt *
Körnerstraße 108, 46047 Oberhausen, Germany

* currently employed at MAN Diesel & Turbo SE, Germany

ABSTRACT

This paper presents the numerical analysis and aerodynamic optimisation of a return channel system and U-turn for multi stage single shaft centrifugal compressor machinery. An optimisation program is used, based on an OpenSource 3D viscous Navier Stokes Solver and an OpenSource evolutionary optimisation algorithm. The coupling between the Navier Stokes flow solver and the evolutionary algorithm is direct, without any meta-model such as ANN (Artificial Neural Network) or a Kriging model. Two different U-turn geometries -based on two different flow inlet profiles- are optimised, analysed and finally coupled to a return channel blade geometry, which is optimised itself. The optimisation of the return channel blade has been set up in two different ways, once with parallel meridional hub and shroud walls and once with a non-parallel optimised meridional shroud contour line. Results show a reduction of total pressure loss by 3% for the optimised blade shapes compared to a standardised blade shape of constant change of tangential momentum. A significant reduction in pressure loss coefficient from 0.825 to 0.627 could be achieved by the optimisation of the meridional contour lines of the return channel. Furthermore, the effect of non-sufficient cross -sectional area at the return channel trailing edge on the overall performance is presented.

NOMENCLATURE

A_5, A_6, A_{av}	Cross sectional area at diffuser, exit, U-turn exit and U-turn passage area [m²]
b_2, b_5, b_6	Blade height at impeller exit, diffuser exit and U-turn exit [m]
c_r, c_Q	Radial and tangential velocity [m/s]
D_2, D_5	Impeller exit diameter, diffuser exit diameter [m]
r_i ,r_6, r_7	Local radius, radius leading/ trailing edge [m]
Ma	Mach number [-]
p_{stat}, $p_{tot,\ inlet}$	Static pressure, total pressure at inlet[Pa]
P	Fraction of flow swirl at return channel exit [-]
Re	Reynolds number [-]
$R_i = r_i/r_6$	Local radius-ratio return channel [-]
$R_7 = r_7/r_6$	Overall radius ratio return channel [-]
s_i	Camberline length [mm]
t	Bezier line parameter [-]
U	Velocity [m/s]
x_i , x_{SS}, x_{PS}	Coordinate camberline , suction/pressure side [m]
y_i , y_{SS}, y_{PS}	Coordinate camberline, suction/pressure side [m]
α_i, α_6	Local absolute flow angle, flow angle at leading edge [deg]
β_i, β_7	Local blade angle, blade angle trailing edge [deg]
δ_i	Blade thickness[mm]
Θ_i	Wrap angle [deg]
ω	Total pressure loss coefficient [-]

INTRODUCTION

Return channel systems (see **Figure 1** for a sketch) are used in multi-stage centrifugal compressor single shaft machinery applied to process industry. The return channel system task is manifold. First, the flow has to be turned from radially outwards to radially inwards, secondly, the flow having a strong swirl due to energy transfer within the centrifugal impeller has to be de-swirled in order to provide vortex-free inlet flow into the following stage downstream. There is strong interaction between the U-turn flow and the return channel blade. Compared to centrifugal impeller and diffuser design, knowledge and open literature for the return channel and U-turn design is rather seldom.

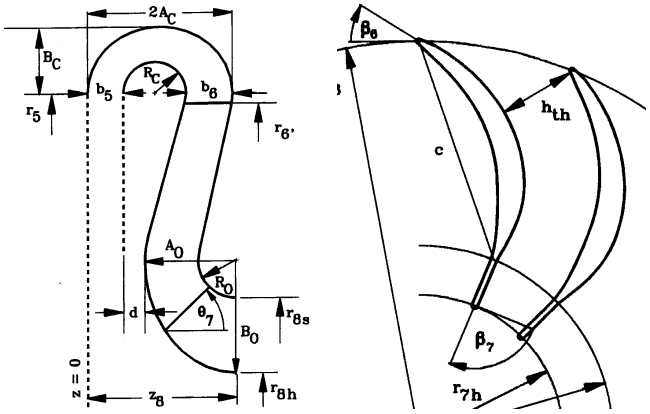

Figure 1 Design sketch from Aungier [9].

History of Return Channel Design

Rothstein [1] made a strong contribution to the understanding of U-turn and return channel flow physics. According to his results, dependent on the curvature of the arc radius, there is a strong influence of the U-turn on the return channel system performance. In the past, a return channel of a multi-stage centrifugal compressor had been inversely designed and optimised [2], [3]. Veress and Van den Braembussche aimed at a smoothed Mach number distribution in order to reduce total pressure loss. This reduced pressure loss was achieved mainly due to extension of the return channel blade into the U-turn. The return channel blade itself was designed with controlled blade loading from leading edge to trailing edge. Recently, the return channel system has gained continuous attention from manufacturers point of view [4]: Aalburg et al. [5] investigated the extension of the stator vane upstream the U-turn in order to reduce total pressure loss and to gain better outlet flow uniformity. Simpson et al. [4] experimentally and numerically applied flow control in a return channel test rig in order to reduce the risk of flow separation in return channel systems of significantly reduced diameter ratio. In Reutter et al. [6], an aerodynamic optimisation of a return channel blade is presented, however based on a more simplified return channel parametrisation which does not allow direct control on the blade angle distribution as presented here. Furthermore, in Reutter et al., a non-

OpenSource CFD code (TRACE) and different optimisation methodology (supported by meta-models such as ANN and/or Kriging) is used. In that specific publication, the optimisation was performed with an impeller exit profile of an industrial impeller (MAN Diesel & Turbo SE) that is not open to public for reasons of non-disclosure agreements. In contrary, the inlet flow profiles presented here, although being generic, mimic general features of centrifugal impeller exit flow well known from literature [7], [8].

When reviewing literature about return channel design, there is no common agreement on, how a well fitted return channel blade should look like. Already for the question of design incidence there exits a variety of different suggestions, whether to allow the flow to slightly (+-2 degree) attack the suction side or the pressure side. In **Figure 1**, a possible design of return channel system is shown as proposed by Aungier [9]. Here, the meridional contours are based on either circular arcs (U-turn hub and L-turn shroud) or ellipses (U-turn shroud and L-turn hub) and Aungier proposes to apply the following design parameters: the passage width b_6 or the flow angle at U-turn exit, the inlet radius r_5 or an area ratio $(A_{av}-A_5)/(A_6-A_5)$ with A_{av} as passage area midway through the U-turn, the hub radius of curvature R_c or the average b/R over the bend. Design specifications of the return channels blade are the vane trailing and leading edge blade angle, and the blade loading parameters which in total specify the vane camberline. Recommendations from Aungier are given for the ratio of passage width to meanline streamline radius of curvature b/R (<1, in average less 0.8). Aungier also proposes front loading near leading edge in order to minimise flow deviation at return channel exit. The vane loading parameters control the loading similar as for impellers and/or vaned diffusers. The flow angle incidence β_6-α_6 should be in a range from 2 to 4 degrees. Pazzi et al. [10] used artificial neural network to study the performance prediction of return channel system. In their study, the diffuser diameter ratio D_5/D_2, the U-turn curvature r/b_2, the return channel blade trailing edge height ratio (b_7/b_6) and the leading edge height ratio b_6/b_2) were investigated, see **Figure 2**. Pazzi et al. concluded that increasing values of U-turn curvature radius r and increasing diffuser ratio D_5/D_2 tend to generally lower the loss coefficient at very low and high values of b_6/b_2, (ratio of blade height at trailing edge to leding edge). For a medium b_6/b_2, there seems to be an optimum in the range of high U-turn curvature r/b_2 at relatively low diffuser diameter ratio D_5/D_2.

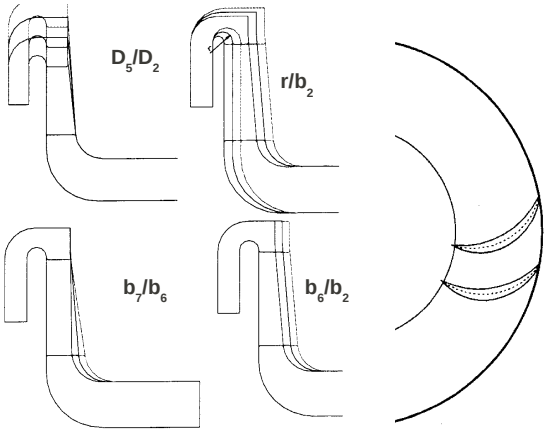

Figure 2 Possible optimisation issues of return channel design according to Pazzi et al. [10]

This minimum loss coefficient probably arises from the matching of flow incidence at the return channel vane leading edge: A lower diffuser diameter ratio results in higher velocity upstream the U-turn which requires to open the leading edge channel height b_5 to match the flow angle to the blade angle. The goal of the optimisation presented in this paper, aims at the specification of an optimised blade trailing edge height ratio (b7/b6), an optimised U-turn meridional contour and an optimised blade shape.

METHODOLOGY

The entire process chain (**Figure 3**) as applied to the optimisation in this paper comprises an evaluation loop in which the return channel systems performance is continuously evaluated by means of 3D-CFD and optimised by an evolutionary algorithm. In the following sub-paragraphs some few features of both the optimiser itself but also the CFD code are presented.

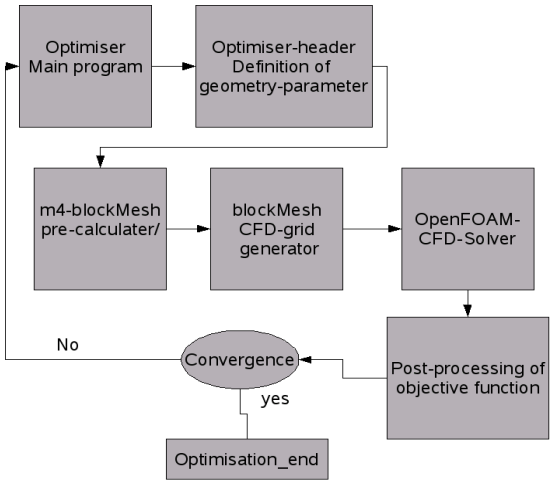

Figure 3 Overview on process chain based on a CFD solver and an optimisation algorithm.

Optimisation-Methodology

There are different kind of optimisation strategies such as gradient based methodology or randomly swarm approach or evolutionary algorithms as used for publication. Shape optimization with adjoint methods have drawn attention to the aerodynamic community, as applied to general shape optimisation [11] or applied to specific turbomachinery components, see Frey et al. [12], and Luo et al. [13]. Frey et al. used this adjoint method for optimisation of a low pressure turbine stator and a transonic compressor rotor. The advantage of adjoint methods over other methods is the reduced calculation effort in the case of optimisation within a large optimisation parameter space. As evolutionary optimisation algorithm, in this paper, also an OpenSource code is used, the so called EO (Evolutionary Optimisation)-sourceforge code, written in C++ originally by the Geneura Team at the University of Granada [14], [15], [16]. EO is distributed under the GNU Lesser General Public License. The code is open for manipulation as necessary in the present task of aerodynamic optimisation. The code features a genetic algorithm based on crossover and mutation of genes. This program implements a simple evolution strategy as defined by Rechenberg and Schwefel: Floating-point chromosome with increments, random selection, random reproduction, with lambda+mu replacement and generational termination. The operators are the standard ones in ES: uniform xover and mutation, which includes mutation of the chromosome value and the sigma. What is left to the users definition is the fitness function, which in the EO-program becomes a fitness function class, the initial population, which in this case is created randomly, and the parameters for mutation and crossover. The relative weights for cross-over and mutation have been set to a default value=0.5 which leaves potential for optimisation of the parameters in future.

Table 1 Parameters of EO-algorithm.

Seed for random number generator:	*50*
Size for tournament selection:	*5*
Number of object variables in genotypes:	*14-29*
Size of population:	*50*
Crossover probability:	*0.8*
Mutation probability:	*0.5*
Range for real uniform mutation:	*0.01*
Std dev. for normal mutation:	*0.3*
Relative weight for hypercube Xover:	*0.5*
Relative weight for segment Xover:	*0.5*
Relative weight for uniform mutation:	*0.5*
Relative weight for det-uniform mutation:	*0.5*
Relative weight for normal mutation:	*0.5*

Against common practise in optimisation of complex evaluation function such as CFD flow field prediction [17], in the present paper, meta-models (Artificial Neural Network, or Kriging) are not used for speed up of the optimisation task. One main reason against these meta-models is in the necessary training task which can be mislead or malfunctioned and secondly in the general mismatch in between these meta-models and the original evaluation model which may lead to miss-orientation for the evolutionary algorithms. In the past, with low computational power, without use of these meta-models, such direct optimisation could not been possible, however nowadays computational power is sufficiently strong (and cheap) for an optimisation with direct evaluation process.

The inlet profile is one key issue for good U-turn and return channel performance. Usually, the impeller exit profile is mainly responsible for the diffuser flow profile. In general, the impeller exit profile is dependent on the quality of impeller design but also on the compressor specific speed and general design questions such as compressor flow coefficient. In Hildebrandt and Genrup [18], the effect of back sweep angle on the impeller outlet flow pattern had been investigated indicating higher flow uniformity for the stronger back sweeped impeller design. In Japikse [19] and Japikse and Osborne [20], total pressure profiles and swirl angles are shown for a specific impeller with and without severe inlet and exit distortions. As is also reported by Rodgers [21], near shroud, the flow profile tends to flatten out, especially in maximum efficiency operation and near choke while towards surge operation, the flow profile seems to be shifted the other way around. The (mass) averaged absolute flow angle level in design point can be nearly linearly correlated with the flow coefficient, as reported in Aungier [9]. In the present paper, the fictive velocity profiles (**Figure 4** and **Figure 5**) refers to this classical flow phenomena of low absolute flow angle at shroud contour downstream the impeller exit due to small meridional velocity component but rather strong circumferential velocity component. The inlet flow profiles are represented by means of Bezier curves of second order being calculated with the formula given below. Four different Bezier curves are connected to each other such that connection is tangential. Each Bezier curve consist of three single control points, called A, B, C.

$$\vec{X}(t)=(1-t)^2\vec{A}+2(1-t)t\vec{B}+t^2\vec{C}$$

The first diffuser inlet flow profile features an averaged absolute flow angle of approximately 33 degree which is a common value for medium to high flow coefficient impellers [9]. The second inlet profile with an averaged flow angle of approximately 22 degree is more of academic interest. This second inlet flow profile is used to check how the optimisation algorithm will adapt the U-turn and the return channel blade to a significantly smaller inlet flow angle with a distributed profile being different to the first inlet profile. An averaged radial velocity of 70 m/s to 90 m/s at impeller outlet is typical for subsonic centrifugal impellers.

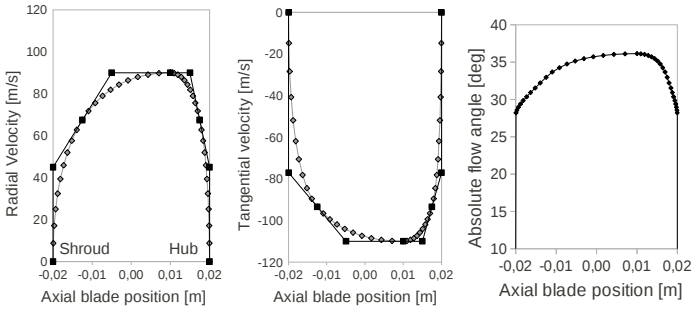

Figure 4 Radial and tangential velocity and flow angle of first inlet profile.

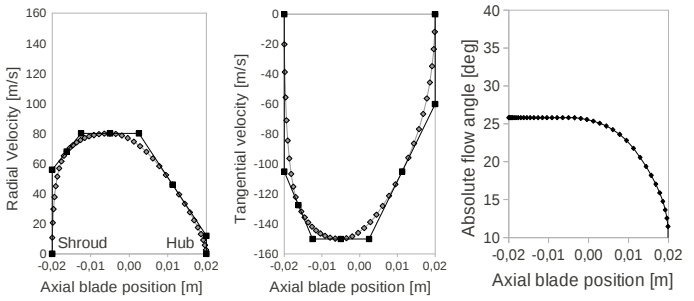

Figure 5 Radial and tangential velocity and flow angle of second inlet profile.

CFD-Grid Generator

The grid generator is based on the OpenFOAM internal blockMesh generator. This grid generator makes use of H-type structered transfinite grid blocking. An additional transcript so called m4-sript is used to allow parametrised blocking by means of vertice, block topology and polyLine definition based on Bezier curves of 2nd order.

CFD-Solver Methodology

As CFD software, OpenFOAM-1.5 (OpenField Operation And Manipulation) is used with the rhoSimpleFoam solver. This Open Source 3D solver features finite volume discretisation for the viscous steady state Navier Stokes equations, combined with a k-ε turbulence model. Model constants of the k- ε turbulence model are standard. Boundary conditions of the calculations are: turbulent intensity = 5%, a total temperature of T_{tot}=345 deg, a velocity profile according to **Figure 4** and **Figure 5** at the inlet and fixed gradient pressure (p_{stat}=200000 Pa) at the exit. According to Japikse and Karon [22], at an impeller exit, lower momentum secondary flow regime may show rather high turbulence levels (up to 15%) while the jet core flow is low turbulent (3%), leading to mean turbulence of approximately 6-8%.

Validation of OpenFOAM

OpenFOAM is recently gaining increased interest from industry's point of view. However, before usage of OpenFOAM as an alternative to commercial software, validation for turbo-machinery with its specific constraints is necessary. Application and validation of OpenFOAM on rotating compressible turbomachinery has not been performed often yet. In the past, OpenFOAM has been used and validated for simple conical diffuser flow [23], [24], where it showed rather good performance of flow field prediction with a classical 2-equation turbulence model. Borm et al. used OpenFOAM for simulation of compressible flow of an axial rotor (NACA-65) profile 2D-simulation, and showed only slight differences in overall pressure ratio (-0.3%) and mass flow (1.9%) to the commercial flow solver NUMECA FineTurbo [25]. Wüthrich [26] simulated compressible nozzle flow by means of OpenFOAM, with satisfactory agreement with experiment data.

As in the optimisation presented here, the geometry of

computational domain does not only apply deceleration in the vaneless diffuser but also imply fluid flow through a U-turn, the author of the present paper additionally evaluated OpenFOAM on the 2D-U-turn NASA test case, reported by Monson and Seegmiller [27], see the Appendix for more information. The results of 2D-U-turn prediction are in good agreement with the experiments. As expected, the RANS modelling has problems to properly predict the flow field at the U-turn exit: In the experiment, the velocity gradient between the core flow and the almost separated flow is stronger than in the CFD prediction.

From the very few open public experimental studies on return channel blade flow ([1],[7]) no sufficient information on the diffuser inlet flow field is unfortunately given such that apropriate CFD validation is not possible. For instance, Rothstein [1] and Inoue et al. [7] do not show the geometrical details on the swirl apparatus nor the flow profile in appropriate distance to the U-turn inlet . By now, to the authors knowledge, there has not been applied any detailed flow analysis by means of Particle Image Velocimetry (PIV), Laser Doppler Anemometry (LDA) or Laser-Two-Focus (L2F) on a test rig with a spinning impeller and return channel system yet. Such kind of measurement campaigns are planned at the RWTH University of Aachen at the Institute of jet propulsion, sponsored by the German Rheinisch Wesfälisch government.

Geometrical Restrictions of Optimisation

Before entering into the results of return channel optimisation, some few words need to be addressed to the comprehension of optimisation. As common in industry in general, there are also limitations from the economical point of view regarding freedom of geometry parameters. By now, mechanical design is restricted to simplified geometries such as a U-turn comprising of circular arcs or a return channel blade that is only designed in two-dimensions and extruded into the third (shaft) direction. Furthermore, a leading and trailing edge at constant radii helps to simplify the process aerodynamic re-design (geometric scaling) to different compressor machinery boundary conditions (hub-tip ratio of shaft, flow coefficient and type of fluid gas) as it is daily process in industrial turbo-machinery design. A two dimensional profile also allows to reduce erroneous results due to wrong CAD/CAM interpretation of ruling surfaces for a three-dimensional blade surface. On the other hand, obviously, the full aerodynamic potential of a return channel blade is not utilised by a two-dimensional design.

2D U-turn OPTIMISATION

For the optimisation of the U-turn, the geometry has been parametrised as mentioned above. The optimisation had been performed on a 2D-grid (see **Figure 6)**, since the flow field has been assumed to be axis-symmetric as to be expected in vaneless diffuser at absence of rotating diffuser stall.

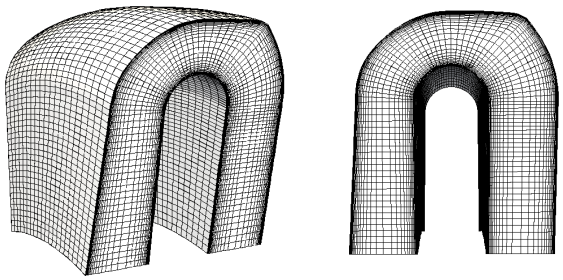

Figure 6: Computational 2D-grid (for better understanding extruded in circumferential direction)

5% turbulence at computational domain inlet has been assumed, the boundary layers had been resolved at an acceptable average y-plus lower than 2. The velocity inlet profile according to **Figure 4** is applied to the inlet of the U-turn computational domain at a radius of 260mm. In order to reduce the total pressure loss in the U-turn, a pinch can be implemented at the end of the diffuser which helps to reduce the risk of flow separation at the outer shroud contour due to concave curvature One optimisation parameter for the specification of diffuser pinch is included in the optimisation. A moderate pinch may help to balance the effects of flow acceleration on the hub and the diffusion of flow on the shroud wall. The optimisation parameters OPT_1 to OPT_6 (see **Figure 7**) were changed in an interval of 0 to 1, while the parameter OPT_7 was allowed to be modified within the range of 0.95 to 1.15. The maximum potential of total pressure loss reduction within the U-turn is rather limited when compared with the return channel system as seen later. Similar as in the case without pinched diffuser design, the turning of flow within the U-turn is rather smooth, the cross sectional area in the second part of the U-turn is slightly increased in comparison with a double circular design. According to the evolution history (see **Figure 7**), the design with minimum total pressure loss is already found after approximately 200 iterations. The reduction of pressure loss of approximately 500 Pa (when comparing to a circular U-turn) corresponds to an increase of isentropic compressor stage efficiency from 82.6% to 83.0% at boundary conditions of (T_{in}=288K, T_{out} =345K, stage inlet pressure =125000Pa).

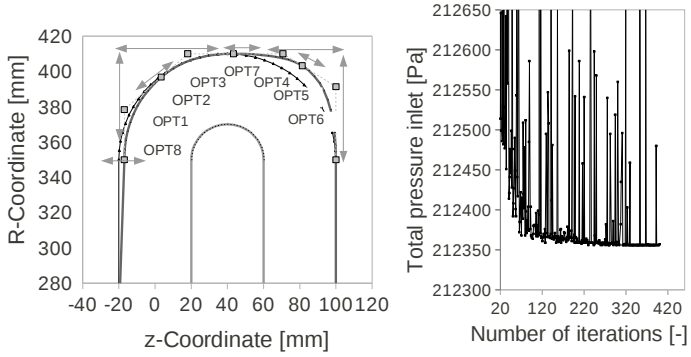

Figure 7 Left: U-turn parametrisation based on 2nd order Bezier curves, right: Evolution history of objective function of one optimisation run.

In **Figure 8**, the evolution of three out of eight optimisation parameters of one optimisation run is presented. When comparing the evolution of these single parameters, one can observe a different behaviour, optimisation parameters OPT_1, OPT_2 (1st part of U-turn) evolve rather fast to their final values, while i.e. the optimisation parameter OPT_7 (2nd part of U-turn) is slower in its evolution and reach a final value range only in the very last 100 iterations. This maybe explained with the evolution of the objective function parameter, the total pressure inlet (see **Figure 7**) which shows its strongest evolution gradient during the first 150 iterations of optimisation.

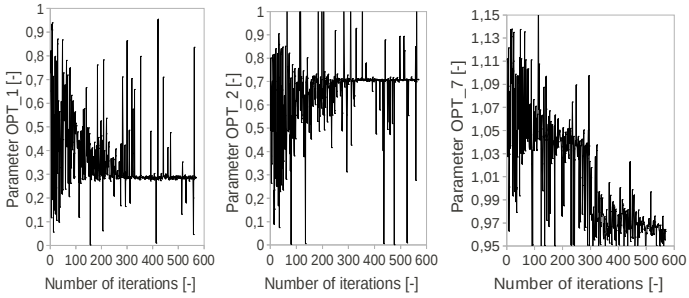

Figure 8 Evolution history of three out of eight U-turn optimisation design parameters.

Obviously, the most potential for good flow turning refers to the 1st part

of U-turn, due to its specific inlet flow profile. which is skewed towards the shroud which is to be optimised. In **Figure 9,** the optimised meridional contour profiles for the two different inlet flow profiles are compared to the classical circular arc. The differences in between the two optimised profiles can be clearly observed: The geometry for the first inlet flow profile shows a reduced concave contour and higher cross-sectional area at the U-turn inlet than the geometry for the second inlet profile since the meridional velocity of the first inlet flow profile is more profiled towards the hub contour. Consequently, as a result of optimisation, the flow profile skewness in this first part of the U-turn is reduced. In the second part of the U-turn, the meridional shroud contour shows stronger bending for the first inlet profile as it helps again, to reduce the deceleration in the outlet section of U-turn (where the hub contour is changed from circular arc to the vertically linear contour) by forcing the flow profile to decelerate already in the part upstream the U-turn outlet. As the second inlet profile is more pronounced towards the shroud contour line resulting in a more uniform meridional flow profile in the entire U-turn, there is no need for such strong bending in the second part of the U-turn shroud as in case of the first inlet flow profile.

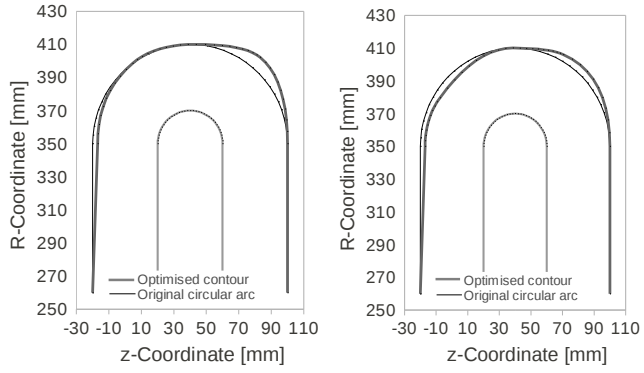

Figure 9 Left: Optimised shroud contour for first flow profile, right: Optimised shroud contour for second flow profile.

In **Figure 10**, the flow angles in one of the optimised U-turns is shown for the first inlet profile. In contrary to the 2D duct without swirl flow and effective passage area width change, the flow angles at the U-turn outlet significantly differ from the U-turn inlet angles. Near the hub, the flow angles do not recover to their original absolute flow angles of approximately 35 degree, even far downstream the U-turn (see right part of **Figure 10** at R=285 mm). As a consequence, the leading edge of a return channel blade being positioned at the outlet of the U-turn (R=350 mm in **Figure 10**) should feature a three dimensional shape. In contrary, any 2D-design is only a compromise which however has to be take into account due to the still high uncertainty of CFD in prediction of strong swirling and curved duct flow.

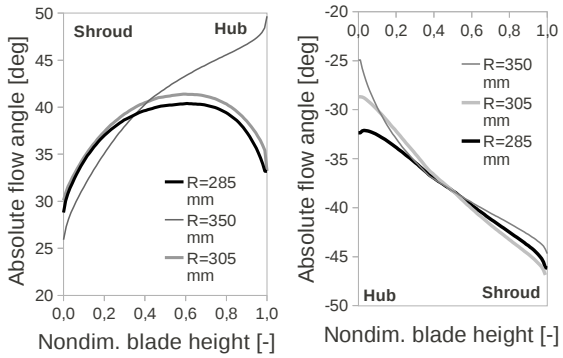

Figure 10 Absolute flow angles (at constant radii) in an optimised U-turn channel system, left: inlet "leg" of U-turn. Right: outlet "leg" of U-turn.

RETURN CHANNEL SYSTEM OPTIMISATION

Blade Geometry Generation

The local blade thickness $\delta_i(r_i)$ and the blade angle distribution $\beta_i(r_i)$ (see **Figure 11**) are calculated via the Bezier control points being selected by the automatic optimisation algorithm. As it is assumed that the return channel blade is two-dimensional and not twisted, the z-coordinate is defined via the outlet z-coordinate of the last point of the U-turn on both the hub and the shroud. The hub and shroud contour of the return channel blade are connected with ruling surfaces. The blade angle being defined as a function of radius, is transformed into the function of x and y-coordinates of the suction ($x_{SS,i}$, $y_{SS,i}$) and pressure side ($x_{PS,i}$, $y_{PS,i}$), see Eq. (2) in **Figure 11**.

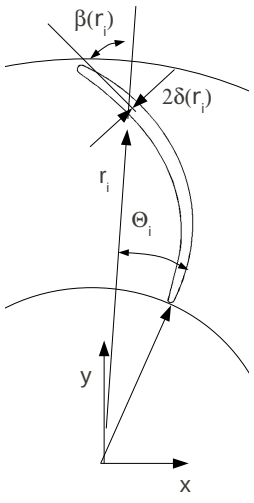

$$dr_i = r_{i+1} - r_i \quad \in (1,n)$$
$$\beta_i = \beta_{i(r)}$$
$$\delta_i = \delta_{i(m)}$$
$$ds_i = dr_i / \tan(\beta_i)$$
$$d\phi_i = ds_i / r_i$$
$$\theta_{i+1} = \theta_i + d\phi_i \quad Eq.(1)$$

$$x_i = -\sin(\theta_i) r_i$$
$$y_i = +\cos(\theta_i) r_i$$
$$dx_i = x_{i+1} - x_i$$
$$dy_i = y_{i+1} - y_i$$
$$d(xy)_i = \sqrt{dx_i^2 + dy_i^2}$$
$$\beta_{(i,x,y)} = \arccos(dx_i / d(xy)_i) \quad Eq.(2)$$

$$x_{SS,i} = x_i - \cos(\beta_{i,(x,y)})\delta_i$$
$$y_{SS,i} = y_i + \sin(\beta_{i,(x,y)})\delta_i$$
$$x_{PS,i} = x_i + \cos(\beta_{i,(x,y)})\delta_i$$
$$y_{PS,i} = y_i - \sin(\beta_{i,(x,y)})\delta_i$$

Figure 11 Return channel blade geometry definition.

The circular arc U-turn has been coupled to a return channel system. A reference design is based on constant/ linear change in the moment of momentum rC_{theta} or linear change in C_{theta}, as has been proposed by Sulaiman [28], see below equation, where the blade wrap anlge Θ_t is calculated by help of the ratio of trailing edge radio to leading edge radius $R_7 = r_7/r_6$ and the radius ratio of local radius to trailing edge radus $R_i = r_i/r_6$.

$$\theta_i = \frac{(R_i - 1)\left[R_7 + R_i\left(\frac{P-1}{2}\right) - \frac{P+1}{2}\right]}{(R_7 - 1)\left[\tan(90 - \alpha_{6b})\right]}$$

P and α_{6b} denote the remaining swirl (in this paper put to 0%) and blade inlet angle, respectively. The leading and trailing edge are designed by means of circular radii such that connection to the remaining blade is smooth in first order (tangential orientation). The computational domain inlet is approximately allocated on a radial height of D=1.1 D_2 downstream a fictive centrifugal impeller.

In order to ensure equal grid quality, the circumferential position of both the periodic boundary conditions relative to the camber line was kept constant. The periodic boundaries were generated by rotating the camberline by +- half a pitch counter and clockwise, respectively. Fourteen full-Blades are used including a meridional contour of constant blade height. The downstream blade height upstream the L-turn had been chosen such that the averaged meridional velocity in the axial outlet should not exceed 150m/s. The diffuser to impeller exit diameter was chosen to be D_5/D_2=700/400, a typical value for an industrial single shaft compressor.

Return Channel Blade Parametrisation

The classical optimisation of return channel systems includes the definition of a L-turn geometry (based on downstream impeller hub/shroud tip ratio), the specification of vaneless diffuser diameter ratio D_5/D_2 (dependent on the degree of reaction of upstream impeller, costs and efficiency), and the curvature radii of the U-turn and L-turn (material cost and rotor dynamic driven factors). For a given return channel blade, the flow incidence at return channel leading edge may be controlled by adaptation of the channel height at leading edge. A general question arises, whether one allows the leading and trailing edge to enter into the meridional curved sections. In this case of optimisation, the leading radius is below the exit radius of U-turn, while the trailing edge is positioned on a radius higher than the inlet radius of downstream L-turn. For the first optimisation, the shape of the meridional contour lines are kept constant, while the blade shape itself is allowed to be modified such that the blade angle distribution and the blade thickness distribution are varied via the corresponding design parameters (Bezier control points to be modified according to the arrows in **Figure 12**). For the optimisations in the following chapters, nine parameters describe the blade thickness distribution and the nine parameters specify the blade angle distribution according to Eq.(1) and (Eq2). The parameters are varied in a range from 0-1 as real figures.

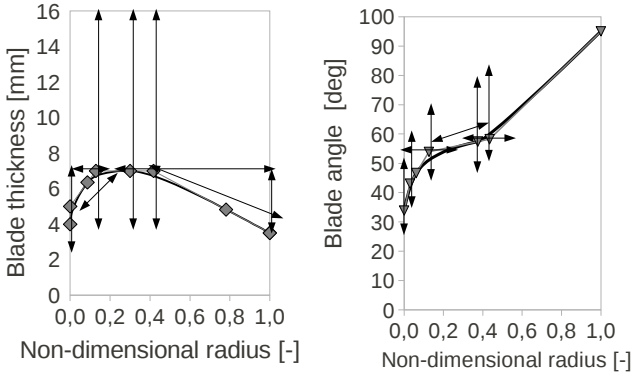

Figure 12 Parametrisation of return channel blade thickness distribution (left) and blade angle distribution (right).

Two different grid sizes were taken for the calculations, one coarse grid (appr. 130,000 cells) for the optimisation runs and a second finer grid (appr. 460,000 cells) for the analysis as presented in the following chapters, see **Figure 13**.

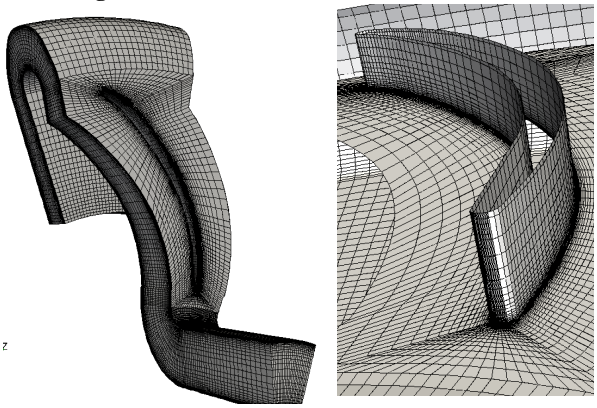

Figure 13 CFD- calculation grid topology, 460.000 cells, for analysis.

To demonstrate the variety of blade shapes that are possible, in **Figure 14**, two examples of very different geometry and one of the best examples of the optimisations are shown in comparison. All kind of loading types and also non-linear changes of camber line and blade thickness distribution are possible by the parametrisation presented.

Figure 14 Left and middle: two random examples of geometries of generated during the preparation of random base, right: one of best examples being optimised for the run including U-turn optimisation.

Results of First Return Channel Blade Optimisation

For all calculations in this chapter, the first inlet profile for the radial and tangential velocity (see **Figure 4**) has been applied as boundary inlet conditions. In **Figure 15**, for one optimisation run, the evolution of six out of eighteen optimisation parameters for the blade angle distribution and thickness distribution is presented. During the optimisation run at least two different optima are found for the parameters OPT_4, OPT_5 and OPT_6 (Bezier control points in the midsection of the thickness distribution). Their optimum values are found relatively early (approximately from iteration No. 400) during the optimisation run, while the Bezier control points for the blade angle distribution, i.e. parameters OPT_16 and OPT_17 aim at their final value after 600 iterations.

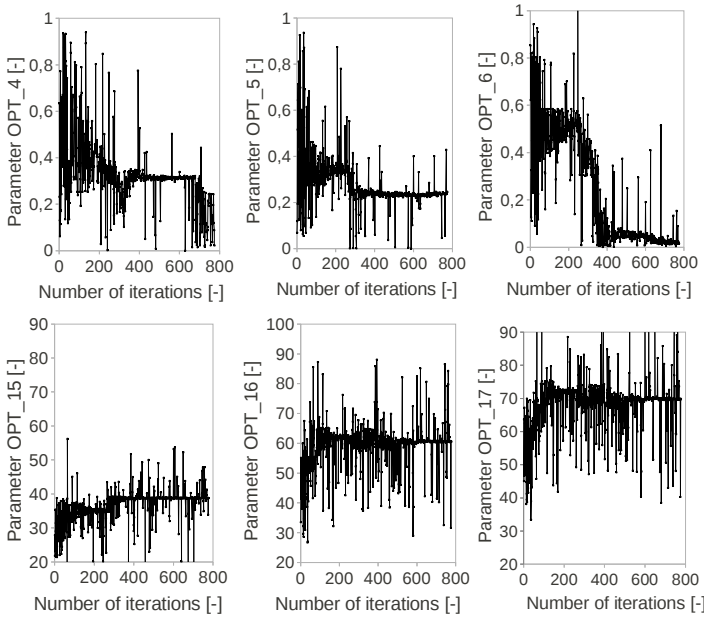

Figure 15 Convergence history of some parameters: Top row: three parameters out of nine from the blade thickness distribution, bottom row: three out of nine parameters of blade angle distribution.

In **Figure 16**, the evolution of the objective function is shown. From approximately 300 iterations on, the gradient of minimisation of the objective function is significantly reduced. After 800 iterations, the optimisation still offers some minor potential for further reduced total pressure drop.

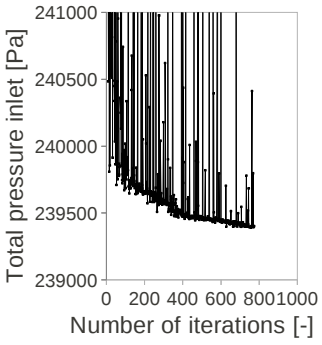

Figure 16 Optimisation run with parallel hub and shroud meridional contour lines (return channel walls): Evolution history of objective function.

Flow Field Analysis

The CFD calculation shows a qualitatively correct representation of potential flow field effects in the S1 blade to blade section due to blade geometry curvature. According to theory, stream-wise passage vortices are generated due to low energetic fluid in the hub and shroud wall boundary layers of the return channel blade system [19]. These stream-wise passage vortices turn from the pressure side to the suction side, especially on the hub as can be seen in **Figure 17.** Here, the additional moving boundary layer flow from hub to shroud can be recognised which is caused by the potential flow field pressure gradient in the downstream L-turn, see the right part of **Figure 17.**

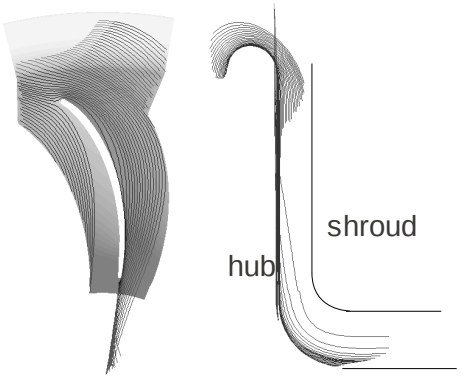

Figure 17 Optimised return channel blade based on boundary conditions of first inlet flow profile: Flow stream-traces (originating near the hub leading edge) in the blade to blade view (left) and meridional view (right).

In **Figure 18**, the effect of the upstream U-turn is clearly seen in the return channel blade to blade section. Near the hub, the Mach number magnitude is significantly reduced. From the Mach number distribution distribution near the hub, a different flow incidence can be observed. Here, due to strongly increased radially directed velocity, flow incidence is towards the suction side. This different flow incidence across the leading edge may give reason for a three dimensionally twisted return channel blade, as has been investigated in Aalburg et al. [5]. However, a 3D-return channel blade is more challenging to manufacture and to design in daily business, especially, when a so-called phi-flowcut methodology is adapted to a base return channel design. This phi-flowcut methodology describes the way to adapt a specific compressor design to different flow media and flow coefficients by keeping the blade shape but reducing the blade height, as it is common in daily compressor design in process industry.

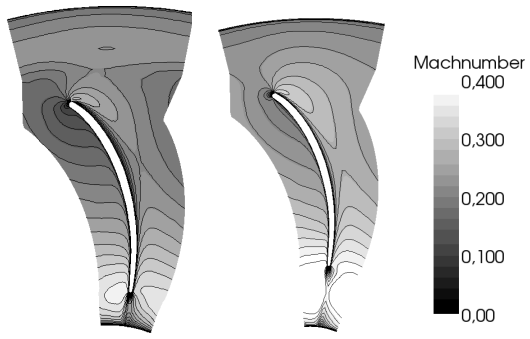

Figure 18 One of best optimised profiles for the case of parallel hub and shroud meridional contour lines. Left: Near hub, right: 50% span.

In order to better understand the flow behaviour of the optimised blade, in **Figure 19**, the absolute flow angles from tangential direction within the return channel blade (optimised blade shape) at different constant radii are shown. At the inlet of the return channel system (r=350mm), the absolute flow angle is skewed due to the potential effect of the U-turn, also a slight potential effect of the leading edge across the circumferential direction can be observed. Within the return channel system at constant radius R=250mm and R=200mm, the core flow does not properly follow the return channel blade angle yet, its flow angle being some few degree higher than at the suction and pressure side. At R= 150 mm near trailing edge, the flow shows significant deviation from blade angle up to six degrees, especially near the suction side. Downstream the trailing edge, the flow is only profiled from hub to shroud, but almost uniform in tangential direction in the mid and shroud section.

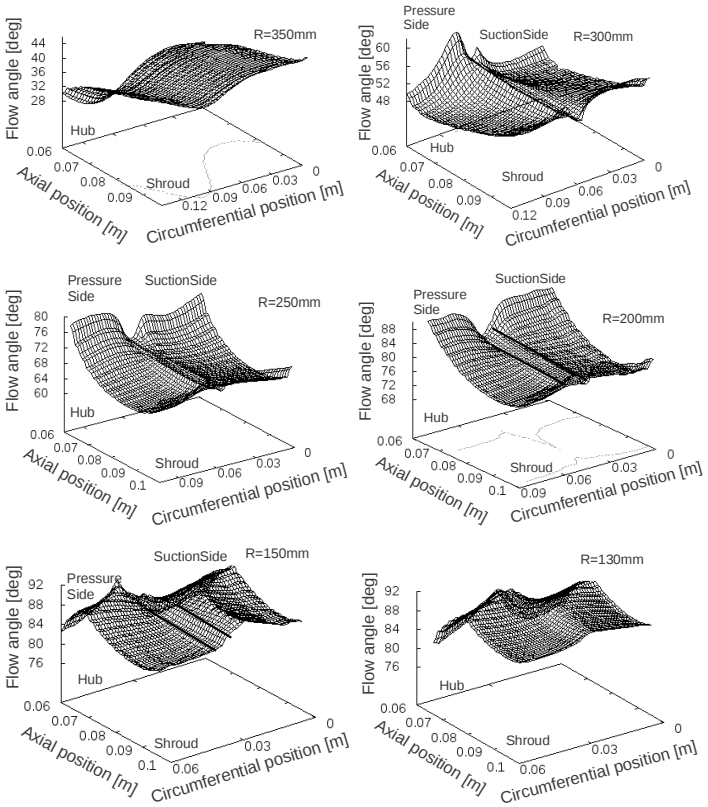

Figure 19. Absolute flow angles at different radii for the geometry with optimised blade shape and parallel meridional hub/ shroud contour lines. Blade angles are β(R=300mm)=54.7 deg, β(R=250mm)=69.8 deg, β(R=200mm)=80.7 deg, β(R=150mm)= 91.5 deg.

In **Figure 20,** the exit flow profile (z=0.25m in axial direction at the outlet of the computational domain) of the optimised return channel and the static pressure distribution of the optimised blade shape are shown. The blade shape shows a very strong pressure reduction along the last third of camber line due to the parallel walls which imply very high velocities at trailing edge and therefore rather high total pressure loss in this section. On the other way, this design results in moderate swirl flow: The absolute flow angle (90 degree = without swirl) only ranges from 82 to 88 degree, with its lower values on the mid channel height. Usually, a remaining swirl of ±10 to ±15 degree is common for return channel blade systems. The wake of the trailing edge is also still evident. Reduced swirl occurs near the hub and shroud walls. This swirl angle characteristics is present in all optimised designs presented so far and could only be counteracted if the blade especially in the region of trailing edge was not based on a 2D or 3D ruling surface design but eventually including a bow design with stronger overturning in the mid-blade height.

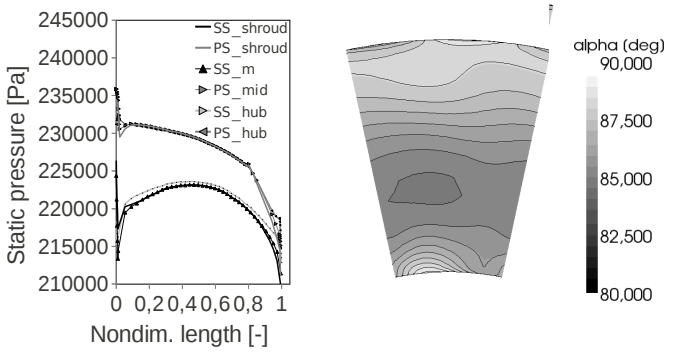

Figure 20 Left: Pressure distribution of the optimised return channel blade (parallel hub and shroud contour lines). Right: Exit flow angle at z= 0.25.

Fully Parametrised Return Channel System

In order to allow more freedom on the parametrisation, but also to avoid the drastic acceleration in the trailing edge section of the return channel blade, an optimisation run was performed that included also the modification of the return channel blade height at leading and trailing edge. Furthermore, a fully Bezier curve-controlled U-turn and a possible pinch to the diffuser by variation of the channel height at diffuser exit were allowed. The absolute Mach number distributions near the hub and at mid channel height (at constant z=0.08m) of one of the best final geometries are shown in **Figure 21**. The strong Mach number increase radially directed towards the trailing edge, as previously seen, is reduced. The optimiser tends to open the return channel height at trailing edge in order to reduce frictional loss.

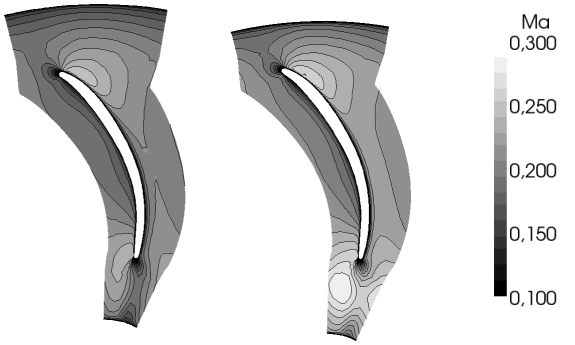

Figure 21 Optimised return channel blade for 1st inlet flow profile. Optimisation set-up including optimisation of U-turn and blade height at leading and trailing edge: Left: Absolute Mach number on 2D slice near hub, right: 2D slice on mid channel height.

During the optimisation (at 460 iterations), it was realised that the optimiser set values of the channel height near the trailing edge at its maximum. Therefore, the corresponding value range was widened, which further reduced the total pressure at inlet by approximately 2000Pa, see also the evolution of this parameter (OPT_28) in **Figure 22**.

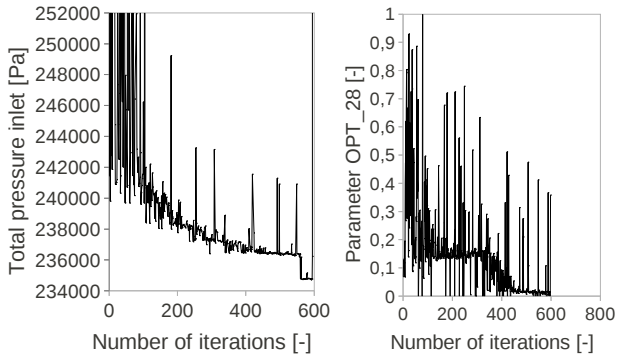

Figure 22 Optimisation run with non-parallel hub/ shroud walls. Left: Objective function (total pressure inlet), right: optimisation parameter for blade height at trailing edge).

The channel height at leading edge is slightly increased to the basic design of constant channel width. Compared to the blade shape with too small blade height at trailing edge, this optimised blade shape looks very different. For the first time the optimiser also intended not to reduce the blade thickness to its minimum value (=4mm) as shown in the previous optimisation runs with the parallel small meridional return channel. In **Table 2**, the overall performance results for the 1st inlet flow profile are presented, indicating a significant reduction of total pressure loss from 0.819 to 0.611 by allowing modification of the return channel meridional blade height. In order to investigate the differences between the optimised and the Sulaiman blade angle distribution, a geometry with the same thickness distribution but adapted constant linear change of tangential momentum has been generated, see **Figure 23** for a comparison of the blade shape- geometry. The blade shape according to the Sulaiman design philosophy provides a total pressure drop being 200 to 300 Pa higher than the optimised blade, independent on whether the meridional return channel contour with optimised or the parallel walls are applied to, see **Table 2**.

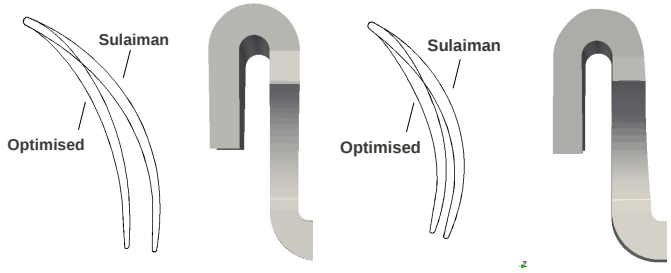

Figure 23 Comparison of blade shapes, left part: Optimised and "Sulaiman" [28] blade with parallel hub/shroud walls, right part: "Sulaiman" blade and optimised blade with optimised hub/shroud walls.

Table 2 Summary of optimisation-overall performance results for the return channel system (from impeller exit to axial outlet downstream L-turn).

Meridional channel contour			*Parallel*	*Parallel*	*Optimised*	*Optimised*
Flow inlet profile [-]			*1st profile*	*1st profile*	*1st profile*	*1st profile*
Blade shape			*Sulaimann*	*Optimised*	*Optimised*	*Sulaiman*
Total_pressure loss coefficient	ω	[-]	0,825	0,819	0,611	0,627
Total pressure inlet	$p_{tot,in}$	[Pa]	238600	238007	233234	233722
Total pressure outlet	$p_{tot,out}$	[Pa]	223849	223402	222560	222741
Static pressure outlet	p_{out}	[Pa]	200000	200000	200000	200000

For the definition of total pressure loss in **Table 2**, the entire computational domain (according to **Figure 13**) from nearly impeller exit to axial exit is taken into account, what explains the relatively high values of total pressure loss. In comparison, the adaptation of a classical blade shape with linear change in momentum (Sulaiman blade) increase the pressure drop comparatively less than the parallel too small channel width. Therefore, before applying an appropriate blade shape, the cross sectional area of the channel has to be specified via 1D calculation. As for the optimised blade with small parallel return channel walls, an analysis of flow angles within the fully parametrised return channel system was performed, see **Figure 24**. According to the enlarged channel width at leading edge, the flow is already in the inlet of the return channel system (R=350mm) directed more tangentially than in the case of parallel walls. Similar qualitative flow features such as strong secondary flow in the hub boundary layers is also observed within this return channel at R=350mm. There is no significant under-turning of the flow at R=200mm. Near trailing edge at R=150mm, however, one can see severe deviation of flow angle from the blade angle in the mid section of blade pitch and blade height. Obviously, the positive effect of less reduced total pressure loss of this return channel system is on account of stronger flow angle deviation due to the relatively weak front-loading of this blade, see also the blade angle distribution in **Figure 26**. As a consequence, the flow is not able to follow the blade turning in the downstream blade section. Finally, the flow deviation is significantly higher than in the case of the optimised blade with parallel walls, compare **Figure 20** and **Figure 25**. In **Figure 25**, also the static pressure distribution of the return channel blade is shown.

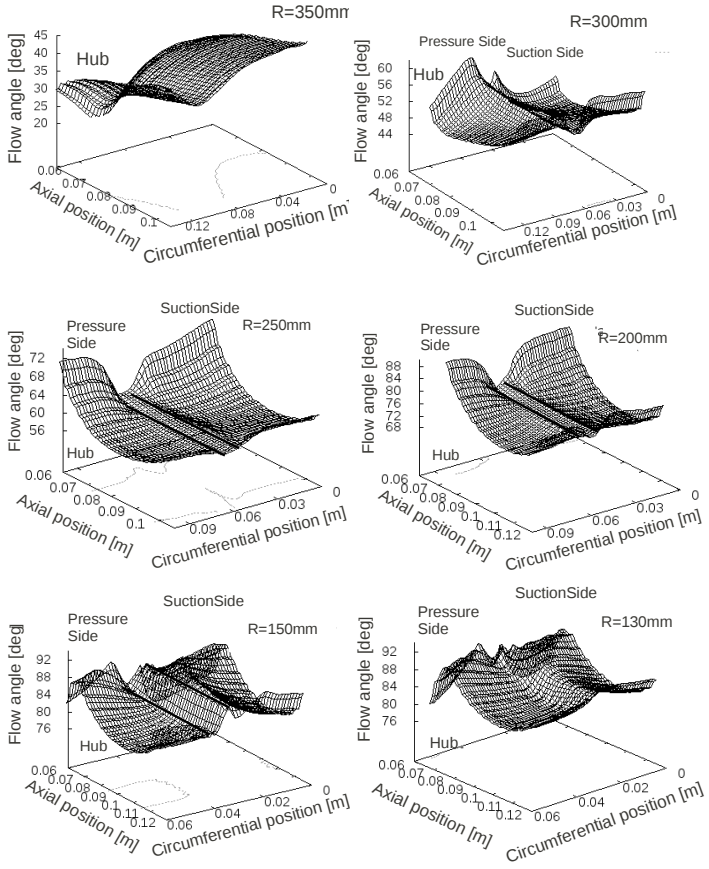

Figure 24 Absolute flow angles at different radii for the geometry with optimised blade shape and non-parallel meridional hub/ shroud contour lines. Blade angles are β(R=300mm)=53.1 deg, β(R=250mm)=59.5 deg, β(R=200mm)=73.9 deg, β(R=150mm)= 90.2 deg

For this optimised blade, the significant drop in static pressure towards the trailing edge is not seen as for the optimised blade shape with parallel meridional hub and shroud contour. When comparing the two different optimised return channel blade geometries, there is a general qualitative overall agreement, such that the blade angle distribution rises monotonously from the leading to the trailing edge, see **Figure 26**. The blade angle distribution of the geometry with non-parallel walls features a similar strong gradient of blade angle in the very first 10% of non-dimensional radius change The inlet blade angle however is nearly the same for both optimised geometries. However, the blade angle distributions from 15% to 100% are significantly different.

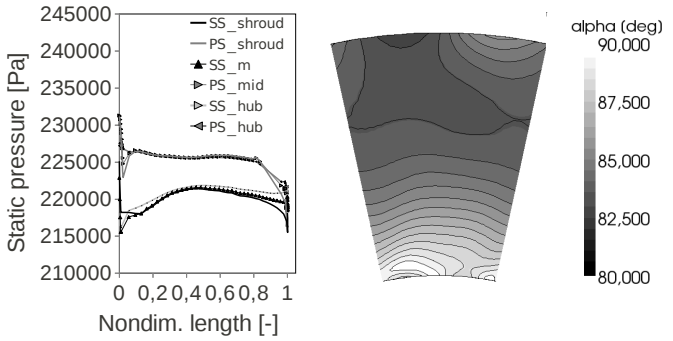

Figure 25 First inlet profile: Left: Pressure distribution of the optimised return channel blade (optimised hub and shroud contour lines). Right: Exit flow angle at z= 0.25.

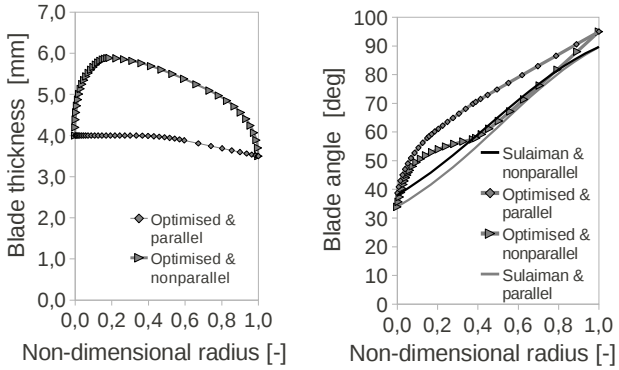

Figure 26 Blade angle and blade thickness distribution of the optimised return channel blade for optimisations with parallel and non-parallel meridional hub /shroud contour lines.

Results of Optimisation for the Second Inlet Flow Profile

In order to check the effect of the flow angle on the optimisation result, a stronger swirl had been applied to the inlet flow profile. For this optimisation, the hub shroud contours are again parallel and not optimised. Corresponding optimised geometries feature an inlet blade angle that is lower by approximately 10 degree compared to the previous geometries with the first inlet flow profile. Furthermore, the increase in blade angle is more linear. For this optimisation, approximately 600 geometries have been calculated, see **Figure 27** for the history of evolution.

In **Figure 28,** the sensitivities of three design parameter are presented. The blade inlet angle was allowed to change from 20 to 40 degree. An optimum is found at around 27 degree. An optimum blade angle at 40% non dimensional radius is given for about 53 degree. Surprisingly, the optimisation objective (low total pressure at inlet) is met for blade inlet angles in range from about 26 to 32 degree. In between this range, the best aerodynamic design is found only in combination

with the remaining parameters. In contrary, the blade angle Bezier control point at 40% non-dimensional height does not vary that much (allowed in range from 20 to 75 degree).

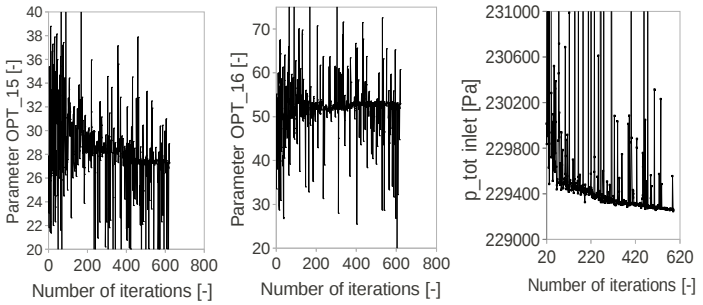

Figure 27 History of evolution of two out of 18 parameters for the second flow inlet profile and the evolution of objective function.

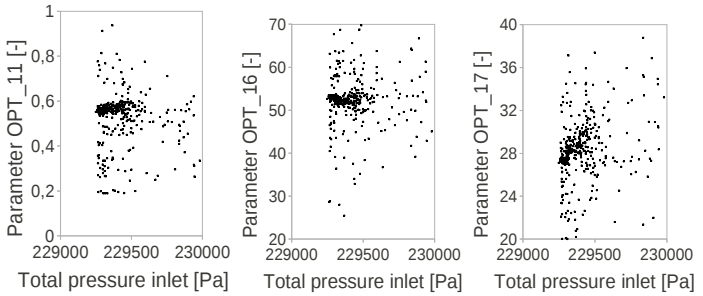

Figure 28 Correlation between design parameter of blade angle distribution: Left and middle: specification of inlet blade angle and blade angle Bezier control point at 40% non-dimensional radius, right: Design parameter near leading edge.

According to **Figure 29**, the blade loading of the geometry for the second flow inlet profile shows a reduction in static pressure loss at 60% non dimensional flow path length due to the parallel hub and shroud walls . The blade loading for the geometry with the second inlet flow profile is relatively front-loaded. For the geometry with the first inlet flow profile and parallel walls, due to over-acceleration in the radial direction towards the return channel blade trailing edge, both suction side and pressure side static pressure tend to lower values than for the geometry with the second inlet profile. In **Figure 30**, for consistency, the blade shape and corresponding total and static pressure for the 2nd inlet profile are shown.

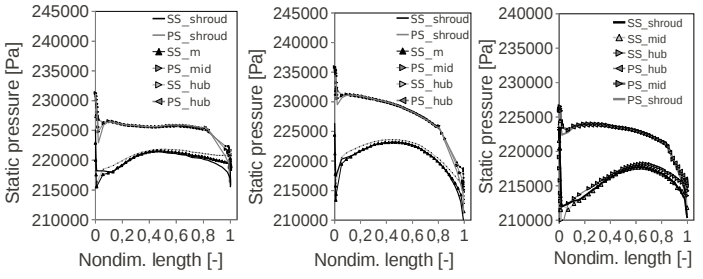

Figure 29 Pressure distribution of three optimised return channel blades: Left: 1st inlet flow profile, non parallel walls, middle: 1st inlet flow profile with parallel walls, right: 2nd inlet profile with parallel walls.

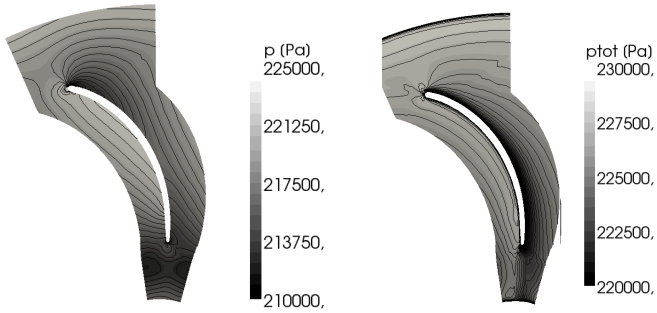

Figure 30 Optimised blade for 2nd inlet flow profile: Static pressure (left) and total pressure (right) in S1 blade to blade plane on 50% height.

Conclusion

A successfully built aerodynamic optimiser has been applied to the design of a centrifugal compressor return channel system to be used in single shaft industrial compressor machinery. The optimisation methodology focussed on a so-called direct method without any meta-modelling for optimisation run speed-up. The optimisation was twofold once aiming at the separated optimisation of the U-turn and secondly at the separated optimisation of the return channel blade. In order to analyse the effect of flow field profile on the optimisation result, two optimisation runs with different flow profiles had been investigated, resulting in a different leading edge angle, a different wrap angle of the return channel blade and consequently a different static pressure distribution. By analysis of the convergence history, sensitive optimisation parameters could be identified which have strong effect on the optimisation result and therefore optimised flow field conditions within the return channel system. In case of the parallel hub/shroud walls, the too small blade height at trailing edge show significantly higher total pressure loss than the optimised shroud contour blade. This concludes, that before entering into time expensive 3D-modelling, also for the return channel design appropriate 1D-modelling has to be applied for. The aerodynamic design in this paper is performed by numerical analysis. Considering the strong curvature effects of geometry and the strong swirling flow of compressible flow (at moderate Mach numbers) one has to keep in mind limitations of CFD-RANS methods [29] in general to properly predict the flow field in return channel systems especially of those with large flow coefficients (being proportional to the volume flow) as has been reported by Lenke and Simon [30]. In future, appropriate validation of CFD predicted return channel flow may seem possible against experimental results of a return channel stage at the RWTH Aachen Institute of Jet Propulsion and Turbomachinery.

ACKNOWLEDGEMENTS

The general OpenFOAM community around Hrvoje Jasak and the OpenFOAM turbomachinery community around Hakan Nilson are highly acknowledged for provision of a CFD-tool being as powerful as commercial CFD-software. Furthermore, the author would like to thank the developers Johann Dréo, Maarten Keijzer, and Marc Schoenauer of the OpenSource optimisation software, which was a key issue for the work presented here. Last but not least I would like to thank Dr. Raik Orbay, for his encouragement and for discussion on general CFD-topics and OpenFOAM in particular.

APPENDIX

Grid Independence Study

Three different grids have been applied to the simulation of the simulation of the return channel system, namely a grid with

approximately 130,000 cells, a grid with 460,000 cells and a grid with 1,000,000 cells. The overall performance results are given in **Table 3**. Small quantitative differences of overall performance between the very dense and medium dense mesh are present but acceptable. Regarding the flow field prediction (not shown here), for the grid with 460,000 cells, the turbulent dissipation profile is a slightly more non-axis-symmetric than for the coarse grid of 130,000 cells. The grid of medium density (460000 cells) also shows slightly higher pronounced velocity on the suction side downstream the return channel leading edge than the coarse mesh. Although the medium dense mesh of 460,000 cells provides a total pressure loss being slightly higher than in the case of 1,000,000 cells it can be concluded that the medium dense mesh almost shows grid independence.

Table 3. Overall performance results of grid independence study.

Cell number			1000000	*460000*	*130000*
Total_pressure loss coefficient	ω	*[-]*	0,587	0,611	0,673
Total pressure inlet	$p_{tot,in}$	*[Pa]*	232696	233234	234773
Total pressure outlet	$p_{tot,out}$	*[Pa]*	222464	222560	222925
Static pressure outlet	p_{out}	*[Pa]*	200000	200000	200000

Evaluation of OpenFOAM on the 2D U-turn NASA Test Case

This NASA test case features a flow through a 2D-U-duct with an inlet bulk velocity of 30.1 m/s at total inlet pressure p_{tot}= 1.2 bar at a normalised inlet total temperature T_{tot}=264.15 K, resulting an a Reynolds number Re=100000. The inlet length of this U-turn is 0.83 m long, the outlet section is 0.540m long, the channel height is 0.038 m and the centerline radius 0.038m, see **Figure 31**. This test Case [27] has also been successfully applied by Rumsey and Gatski [31] as CFD validation concluding that an explicit algebraic stress model provides higher flow prediction accuracy than one -or two equation eddy viscosity models. The OpenFOAM validation results presented here, have been generated with a default k-e model. Although there is some difference between CFD (red lines in **Figure 32** to **Figure 35**) and experiments, especially in the outlet section, in general, the comparison is satisfactory.

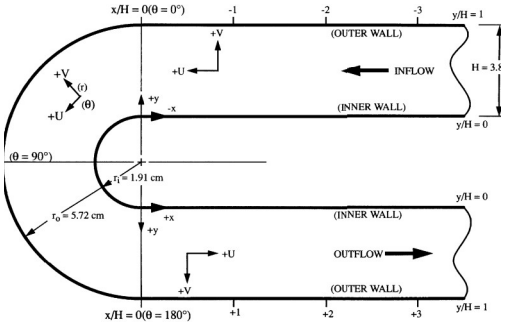

Figure 31 U-turn sketch of 2D-Nasa Test-Case.

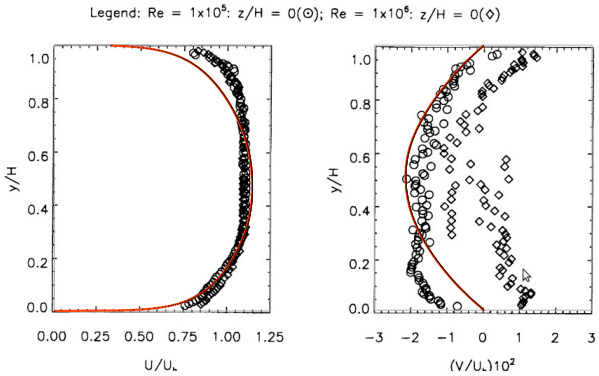

Figure 32 Longitudinal and vertical velocity one channel height upstream U-turn.

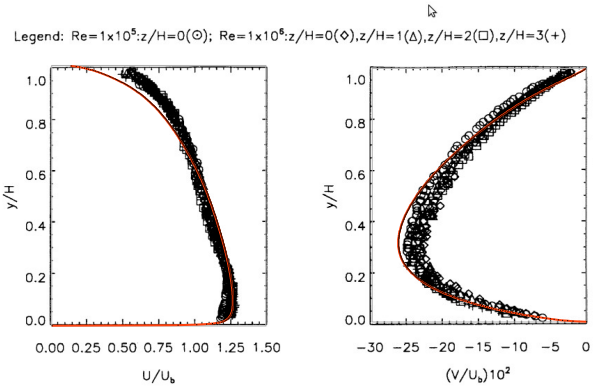

Figure 33 Longitudinal and vertical velocity at inlet of U-turn.

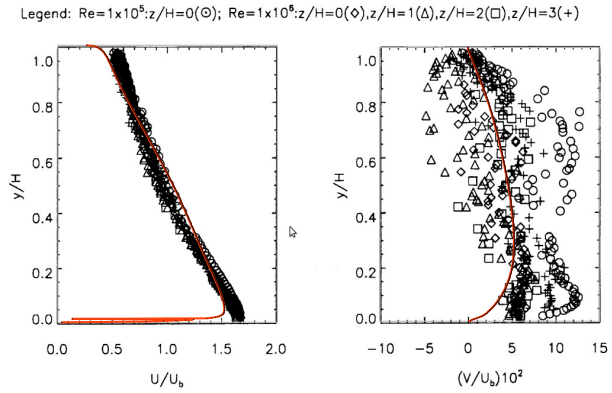

Figure 34 Longitudinal and vertical velocity at 90 deg section of U-turn.

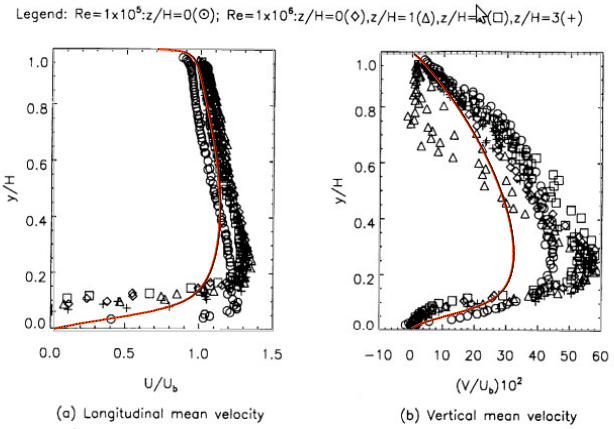

Figure 35 Longitudinal and vertical velocity at outlet of U-turn.

REFERENCES

1 Rothstein, E., 1984, *"Experimentelle und theoretische Untersuchung der Strömungsvorgänge in Rückführkanälen von Radial-verdichterstufen, insbesondere solcher mit geringen Kanalbreiten"*, Fakultät für Maschinenwesen der Rheinisch-Westfälischen Technischen Hochschule Aachen.

2 Toyokura, T., Kanemoto, T., Hatta, M., *„Studies on Circular Cascades for Return Channels of Centrifugal Turbomachinery"*, Bulletin of JSME, Vol. 29, No 255 September 1986.

3 Verres, A., Van den Braembussche, R., *„Inverse Design and Optimization of a Return Channel for a Multistage Centrifugal Compressor"*, ASME Journal of Fluids Engineering, Sept. 2004, Vol. 126.

4 Simpson, A., Aalburg, C., Schmitz, M., Pannekeet, R., Larisch, F., Michelassi, V., *"Application of Flow Control in a Novel Sector Test Rig"*, Proceedings of ASME Turbo Expo 2009, GT2009-60126, June 8-12,

Orlando, Florida, USA.
5 Aalburg, C., Simpson, A., Carretero, J., Nguyen, T., Michelassi, V., *„Extension of the Stator Vane Upstream Across the 180deg Bend For a Multistage Radial Compressor Stage"*, Proceedings of ASME Turbo Expo 2009: Power for Land, Sea and Air, GT2009-59522, June 8-12
6 Reutter, O., Hildebrandt, A., Jakiel, C., Raitor, T., Voss, C., *"Automated Aerodynamic Optimization of a Return Channel Vane of a Multi-stage Radial Compressor"*, to be presented on the European Turbomachinery Conference 2011.
7 Inoue, Y., and Koizumi, T., " *An Experimental Study on Flow Patterns and Losses in Return Passages for Centrifugal Compressors",* Applied Mechanics, Bioengineering and Fluids Engineering Conference Houston, Texas, June 20-22, 1983
8 Benvenuti, E., 1978, *"Aerodynamic Development of Stages for Industrial Centrifugal Compressors. Part 1: Testing Requirements And Equipment-Immediate Experimental Evidence",* ASME Paper No. 78-GT-4.
9 Aungier, R.H., *"Centrifugal Compressors: A Strategy for Aerodynamic Design and Analysis"*, book published by ASME Press, New York, 2000.
10 Pazzi, S., Martelli, F., Vichelassi, V., Giachi, M., *"The Use of Artificial Neural Networks for Performance Prediction of Return Channels for Industrial Centrifugal Compressors"*, Proceedings of ASME Turbo Expo 2002, GT2002-30392, 3-6 June 2002, Amsterdam, The Netherlands.
11 Othmer C., " CFD Topolgy And Shape Optimisation with Adjoint Methods", VVDKi Fahrzeug- und Verkehrstechnik 13. Internationaler Kongress Berechnung und Simulation im Fahrzeugbau, Würzburg, September 2006.
12 Frey, C., Nürnberger, D., Kersken, H.P., *"Development and Application of an Adjoint RANS Solver for Turbomachinery"*, In: Proc. 8th European Conference on Turbomachinery, Seiten 949-958. Eigth European Conference on Turbomachinery, 23.-27. März 2009, Graz, Österreich.
13 Luo, J., Xiong, Jl., Liu, F. and McBean, I., *"Three-Dimensional Aerodynamic Design Optimisation of a Turbine Blade by Using an Adjoint Method",* Proceedings of ASME Turbo Expo 2009: Power for Land, Sea and Air, GT2009 GT2009-60115, Orlando, Florida USA.
14 *http://eodev.sourceforge.net*, dated 10th november 2010.
15 Keijzer, M., Merelo, J.J., Romero, G., Schoenauer, G., M., *"Evolving Objects: A General Purpose Evolutionary Computation Library"*, Art. Evol. 2310, 231-242 (2002).
16 J.J. Gilijamse, J. Küpper, S. Hoekstra, S.Y.T. van de Meerakker, G. Meijer, *"Optimizing the Stark-Decelerator Beamline for the Trapping of Cold Molecules Using Evolutionary Strategies"*, Phys. Rev. A 73, 063410 (2006). Also available at arXiv physics/0603108 (2006).
17 Verstraete, T., Alsalihi, Z., Van den Braembussche, R. A., *"Numerical Study of the Heat Transfer in Micro Gasturbines",* ASME Journal of Turbomachinery, October 2007, **Vol. 129**, Issue 4, pp 835 – 841 .
18 Hildebrandt, A., Genrup, M., *"Numerical Investigation of the Effect of Different Back Sweep Angle and Exducer Width on the Impeller Outlet Flow Pattern of a Centrifugal Compressor With Vaneless Diffuser"*, ASME Journal of Turbomachinery, April 2007, **Vol. 129**.
19 Japikse, D., *„Centrifugal Compressor Design and Performance"*, Concepts ETI, Inc, 1996.
20 Japikse, D, Osborne, C 1986, *"Optimization of industrial centrifugal compressors, Part 6B: Studies in component performance- Laboratory development of eight stages from 1972 to 1982"*. ASME Paper No. 86-GT-222.
21 Rodgers, C., *"The performance of centrifugal compressor channel diffusers"*, ASME Paper No. 82-GT-10, 1982.
22 Japikse, D., Karon, D., M., *"Laser Transit Anemometry Investigation of a High Speed Centrifugal Compressor"*, ASME paper No. 89-GT-155.
23 Nilsson, H., Page, M., Beaudoin, M., Gschaider, B., and Jasak H., *"The OpenFOAM Turbomachinery Working Group, and Conclusions from the Turbomachinery Session of the Third OpenFOAM Workshop",* 24th IAHR Symposium on Hydraulic Machinery and Systems, October 27-31, 2008, Foz Do Iguassu, Brazil.
24 Bounous, O.,. *"Studies of the ERCOFTAC Conical Diffuser with OpenFOAM"*, Research Report 2008:05, Applied Mechanics, Chalmers University of Technology, Sweden, 2008. Presented at the Third OpenFOAM Workshop in Milano, July 9-11, 2008.
25 Borm, O., Balassa, B., Barthmes, S., Fellerhoff, J., Kührmann, A., Kau H.-P., *"Demonstration of an Aerodynamic Design Process for Turbomachines Using OpenSource Software Tools"*, Proceedings of ASME Turbo Expo 2010, Power for Land, Sea and Air, June 14-18, Glasgow, UK, ASME Paper No. GT2010-22194.
26 Wüthrich, ,B., *"Simulation and Validation of Compressible Flow in Nozzle Geometries and Validation of OpenFOAM for this Application"*, Computational Science and Engineering MSc ,Master Thesis SS 07 Institute of Fluid Dynamics , ETH Zurich , Written at ABB Corporate Research Baden-Dättwil
27 Monson, D.J., and Seegmiller, H.L., *"An Experimental Investigation of Subsonic Flow in a Two-Dimensional U-Duct"*, NASA TM 103931, July 1992.
28 Sulaiman, A. T., *„Investigations Into the Return Channel for Multistage Centrifugal Pumps"*, Department of Mechanical Engineering, Paisley, College of Technology, Scotland, 1975.
29 Gianluca, Iaccarino, *„Predictions of a Turbulent Separated Flow Using Commercial CFD Codes",* ASME Journal of Fluids Engineering December 2001, ol. 123 /819-828,
30 Lenke, L.J., Simon, H.,*"Numerical Investigations within Return Channels of Multi-stage Centrifugal Compressors"*, VDI-Berichte Nr. 1425, 1998.
31 Rumsey, C.L., Gatski, T.B., *"Turbulence Model Predictions of Extra-Strain-Rate Effects in Strongly-Curved Flows",* AIAA 99-0157, 37th Aerospace Sciences Meeting & Exhibit, , Reno, Nevada, US, January 1999.